International Journal of Fluid Power 9 (2008) No. 3 pp. 45-53

AIR BEARING TESTING

Federico Colombo and Andrea Trivella

Dept. of Mechanics, Politecnico di Torino, C.so Duca degli Abruzzi 24, 10129 Torino, Italy
federico.colombo@polito.it , andrea.trivella@polito.it

Abstract

This article provides an overview of experimental air bearing testing at the Politecnico di Torino Department of Mechanics. The types and design features of the air bearings investigated at the Department are illustrated together with the test benches and instrumentation used to determine their performance. Several examples of the experimental results obtained through this work are presented.

Keywords: pneumatics, air bearings, air pads, test bed

1 Introduction

Air bearings consist of two elements in relative motion separated by a thin film of pressurized air a few dozen microns thick. The phenomena that govern the operation of these devices are well known, and their applications are numerous.

In fluid lubrication these components are used when the following are required: low friction and power loss, high precision in positioning, and ultra high rotational speeds.

As they are free from contaminants if supplied with clean air, air bearings and pneumatic guideways are often used in the food processing, textile and pharmaceutical industries. They are also found in small machine tools and measuring robots, in the microturbines used for distributed electricity generation, and in the gyroscopes employed in inertial navigation systems. Another emerging application is that of high-speed compressors for fuel cell systems.

Because of the extremely close manufacturing tolerances that air bearings require and the lack of standard large scale production models, their costs are by no means competitive with those of the rolling bearings in common use. Initial investments must be evaluated case by case to determine whether they will be outweighed by the savings that result from these bearings' near-negligible maintenance and freedom from wear, which makes their service life practically unlimited.

A large number of investigations of air bearings have been conducted using experimental, numerical and theoretical approaches with analytical models, e.g. Boffey and Desai (1980), Boffey and Wilson (1981) and Czolczynski (1994). Nevertheless, work must still be done to improve stiffness, load capacity and stability. Potential designs are studied individually, seeking to meet the major requirements for the particular application with as little influence on the others as possible. For dynamic air bearings, applications are currently limited to those involving low power, though an increasing amount of work is focusing on developing reliable solutions for higher-power uses. Machine tool applications, for example, call for stiffnesses comparable to those of the rolling bearings in current use, while operating stability must be guaranteed at the highest rotational speeds. In such cases, parameters such as the number and diameter of supply holes, their arrangement, and supply system geometry come into play. Where rotor stability under low load at very high rotational speed is the prime consideration, designs can be adopted which bring rotor orbit amplitude down to acceptable levels.

Numerical calculation can assist bearing design, but its validity must be verified through basic experimental investigations.

The research group composed by G. Belforte, F. Colombo, T. Raparelli, A. Trivella and V. Viktorov studies air bearing systems at the Politecnico di Torino Department of Mechanics. The activity concerns the "High Speed Rotor and Bearing Laboratory" that is part of the IBIS HQL project. This paper presents the experimental activity of the group, in particular the test benches designed and used for experimental activity. The air bearings investigated and constructed are pre-

This manuscript was received on 3 June 2008 and was accepted after revision for publication on 15 October 2008

sented below, together with the test benches used to assess them. First to be discussed will be aerostatic bearings and several methods for increasing their stiffness, followed by variable-profile pneumatic guideways. The article will conclude with the Department's work with dynamic air bearings. For all types, experimental testing was carried out in parallel with theoretical studies employing analytical and numerical models.

2 Aerostatic Bearings

The load capacity and stiffness of air bearings is heavily influenced by supply system geometry. To investigate its effects, a number of cylindrical aerostatic pads were constructed. All pads had the same outside dimensions but featured supply systems that differed in type and geometry. By way of example, Fig. 1 shows schematic views of pads with an annular orifice supply system (type *a*), and pads consisting of a simple orifice with feed pocket supply system (type *b*), see Belforte et al. (2006A) and Belforte et al. (2007C). For type *a* systems, several pads were constructed whose single central hole had different diameters and lengths (d = 0.2, 0.3, 0.4 mm; l = 0.3, 0.6, 0.9 mm). For type *b* systems, designs b_1 and b_2 were constructed. Type b_1 is a pad with a single central hole, while type b_2 had six holes equally spaced around the circular face. Interchangeable drilled inserts can be installed on both pad designs; for type b_1, the feed pocket has a diameter d_0 = 2 mm and depth δ = 1 mm, while for type b_2 d_0 = 4 mm and feed pocket depth δ can be varied.

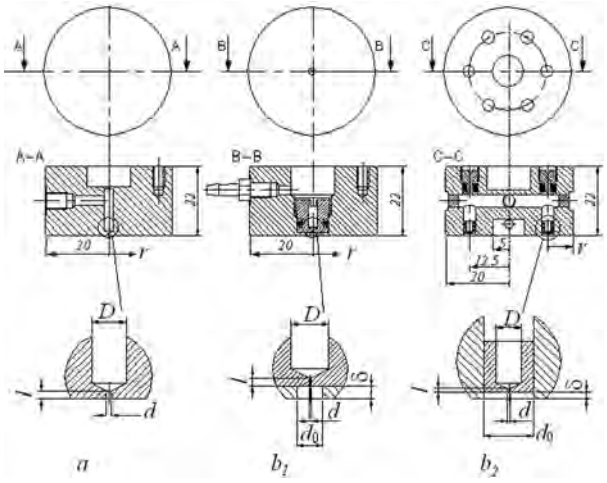

Fig. 1: *Air pads with different supply systems, a: annular orifice; b_1, b_2: simple orifice with feed pocket*

Configurations of type b_2 pad with d = 0.2, 0.3, 0.4 mm and δ = 10, 20, 30 μm were tested. With the same pad further investigations were conducted whose supply inserts were connected by a 30 μm depth and 0.8 mm wide circumferential groove.

Figure 2 shows alternative supply systems with resistances consisting of different types of porous media: sintered metal powders (type *c*), see Belforte et al. (2007B) and fine-mesh woven wire cloth (type *d*), see Belforte et al. (2007A). In the first case, several cylindrical sintered bronze porous resistances with different diameters and particle sizes were housed in inserts installed in the pad. In the second case, the inlet resistance was produced using several types of commercial woven wire cloth with different porosity.

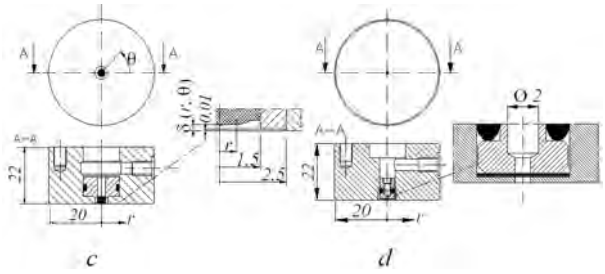

Fig. 2: *Air pads type c : with sintered powders; d : with metallic mesh*

For both designs, interchangeable resistances could be installed on each pad, which features a central supply hole and a pocket between the resistance and the air gap. The photograph in Fig. 3 shows the pads constructed for each type, viz.: annular orifice *a*, simple orifice with feed pocket and circumferential groove *b*, sintered metal powders *c*, and woven wire cloth *d*.

A schematic view of the test set-up used for measuring aerostatic pad static load capacity, stiffness, pressure distribution and air consumption is shown in Fig. 4. The set-up frame consists of a base (1), three columns (2) and a crossmember (3). The air gap is established between the pad under test (4) and the stationary bearing member (14). The height of the air gap is measured by three micrometric transducers (6).

Pad movement is accomplished by means of a screw (7) controlled by handwheel (8), pushrod (9) and ball (10) housed in plate (5), which is positively connected to the pad (4).

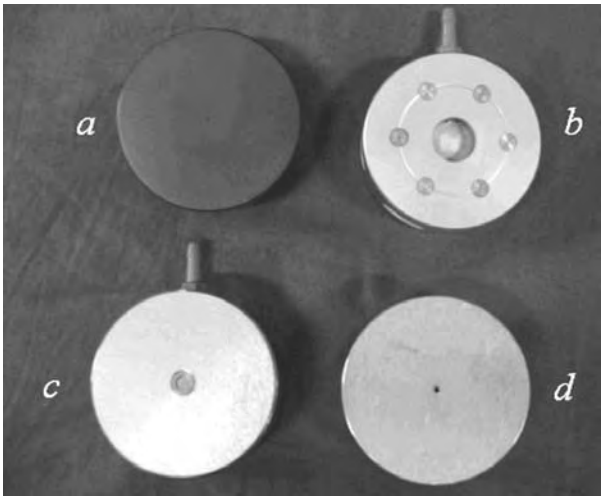

Fig. 3: *Air pads with different supply systems: a, annular orifice; b, simple orifice with feed pocket; c, porous resistance; d, fine metallic meshes*

Thrust on the pad is measured by a load cell (11). Pad angle can be adjusted as necessary using two screws (13). The stationary bearing member (14) makes it possible to determine pressure distribution below the pad, as it is provided with two holes connected to pressure transducers, and can be moved radially with respect to the pad.

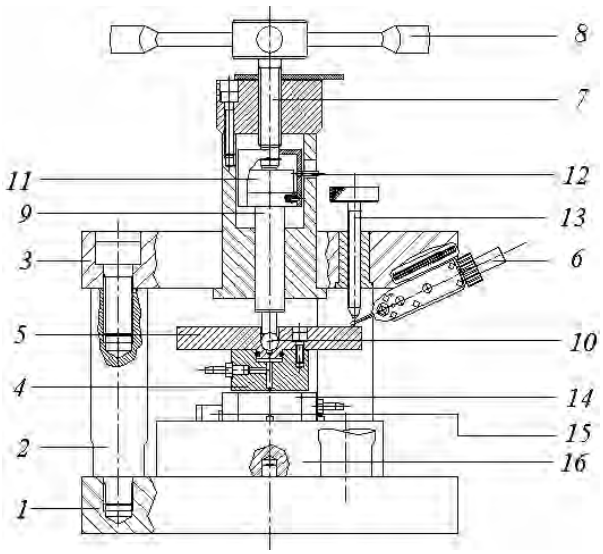

Fig. 4: *Sketch of the air pads test bed*

A photograph of the test set-up is shown in Fig. 5. By way of example, the graphs in Fig. 6 and 7 show pressures along the air gap measured for the annular orifice supply system and simple orifice with feed pocket respectively, with relative supply pressure p_S = 0.5 MPa and air gap heights h of 9 and 14 μm.

Fig. 5: *Photo of the air pad test bed*

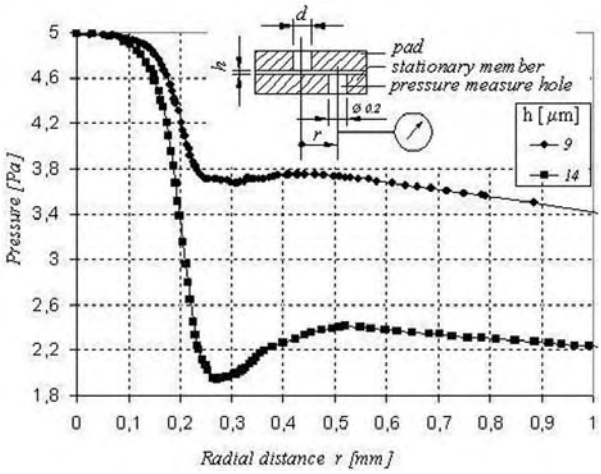

Fig. 6: *Radial pressure distribution across the pad type a, supply pressure p_S= 0.5 MPa, orifice diameter d = 0.2 mm, air gap height h = 9 and 14 μm*

For these systems, pressure distribution and mass flow rate measurements were used to calculate hole discharge coefficients C_d as a function of air gap height and supply pressure.

The aerostatic journal bearing for linear motion constructed is shown schematically in Fig. 8. (1) is the journal, (2) is the bearing of diameter D = 50 mm and axial length L = 60 mm, provided with four equally spaced air inlet holes of diameter d_B = 0.4 mm. The radial air gap is designated as h; and when journal and bearing are coaxial, $h = h_0$ = 20 μm. Each hole communicates with a pocket of axial length L_p = 44 mm, width a = 15 mm, and depth δ = 100 μm. Bearing mass is 1.6 kg.

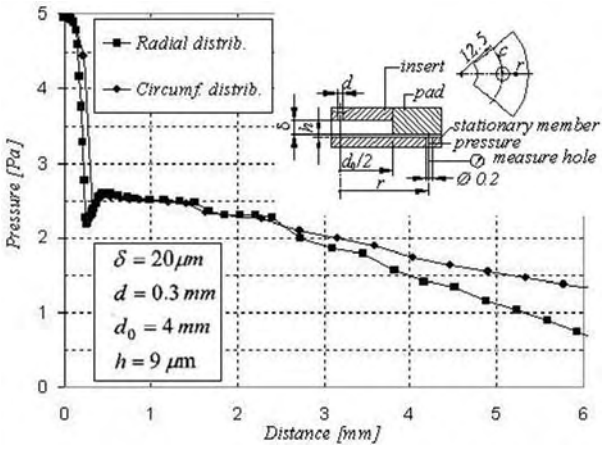

Fig. 7: *Radial and circumferential pressure distribution across the pad type b, supply pressure p_S= 0.5 MPa, orifice diameter d = 0.3 mm, pocket diameter d_0 = 4 mm, pocket depth δ= 20 μm, air gap height h = 9 μm*

An application of this type of bearing is shown in the photograph of Fig. 9.

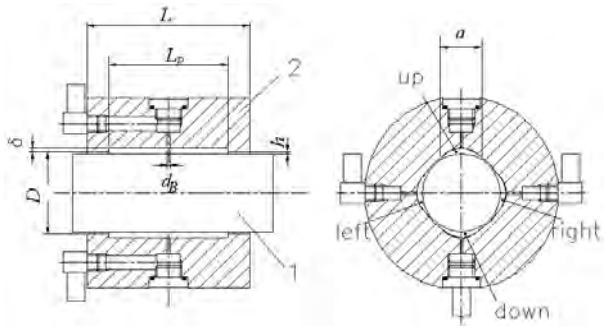

Fig. 8: *Sketch of a pneumostatic bearing*

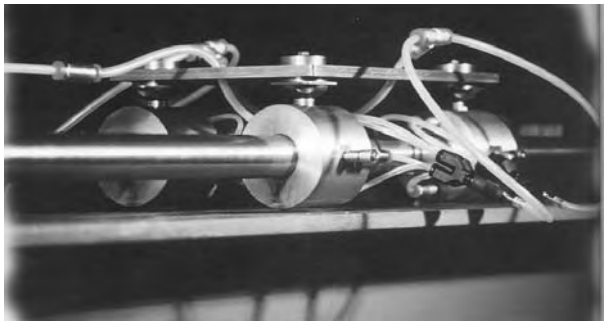

Fig. 9: *Slide composed of gas bearings*

A test bench for measuring the stiffness of aerostatic journal bearings is shown schematically in Fig. 10, see Raparelli et al. (1998).

Journal (1) is secured to the frame and coupled to bearing (2). Relative rotation between journal and bearing is prevented by means of a pneumatic guide (3) positively connected to the frame; a shaft connected to the bearing runs vertically in the guide. Rod (7) connected to the lower portion of the bearing makes it possible to apply one or more calibrated weights (8) to plate (9). The ball joint on the shaft is used to eliminate the horizontal force components. The end of the shaft faces the inductive sensor (5) used to measure the vertical bearing movement. The air supply (10) maintains a small compensation reservoir (11) under pressure, crossing a high-efficiency filter (12) to reach supply pressure reducers (13) (14) (15).

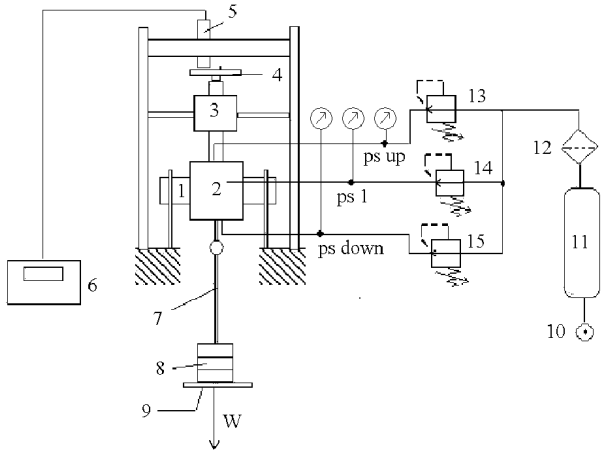

Fig. 10: *Sketch of pneumo-static journal bearing*

2.1 Actively Compensated Aerostatic Bearings

To increase the stiffness of the aerostatic journal bearing described above, position control systems were developed which vary bearing supply pressures. An electronically controlled type is shown in Fig. 11.

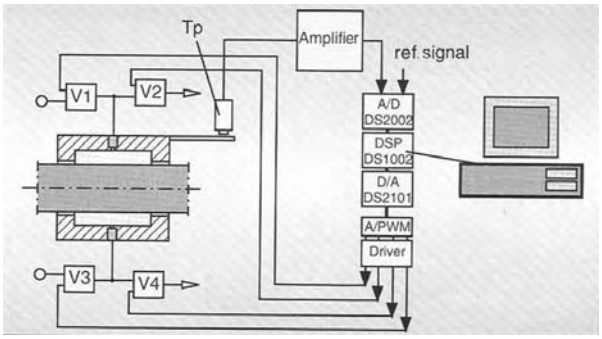

Fig. 11: *Electronically controlled air bearings*

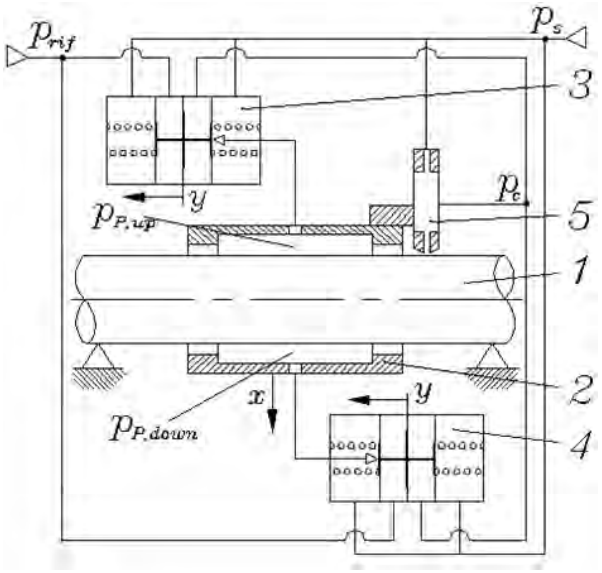

Fig. 12: *Pneumatically controlled air bearings*

Inlets to the top and bottom bearings are connected to supply or to discharge via digital PWM modulated solenoid valves V_1 and V_2. The valves make it possible to achieve a continuously variable conductance and are driven by a control system that compares a reference signal with the signal from inductive position transducer T_p.

An all-pneumatic control system has also been developed as an alternative to this design, see Raparelli et al. (2000). The system is represented schematically in Fig. 12, which shows journal (1), bearing (2), two compact pneumatic proportioning valves (3) and (4) connected to the top and bottom bearing inlets and a displacement sensor (5) for the feedback signal. The valves and the sensor were designed specifically for the control system. With supply pressure and in absence of external load the bearing is coaxial with the journal, reference pressure p_{rif} is equal to displacement sensor output pressure p_c and the pressures inside the pockets are the same. When a vertical load is applied, pressure p_c changes, the mobile elements of the valves displace,

thus increasing/decreasing the supply pressure in the relative inlets of the bearing. In this way, a self-centering force is generated, which tends to maintain the bearing in a coaxial position.

Figure 13 is a photograph of the test bench constructed for this system. The graph in Fig. 14 shows bearing vertical displacement from the coaxial position versus applied load for passive operation, actively compensated operation with electronic control, and actively compensated operation with pneumatic control. In particular, pneumatically controlled active compensation was achieved by opening out the bearing supply holes at the top and bottom inlets to a diameter d_B = 3 mm.

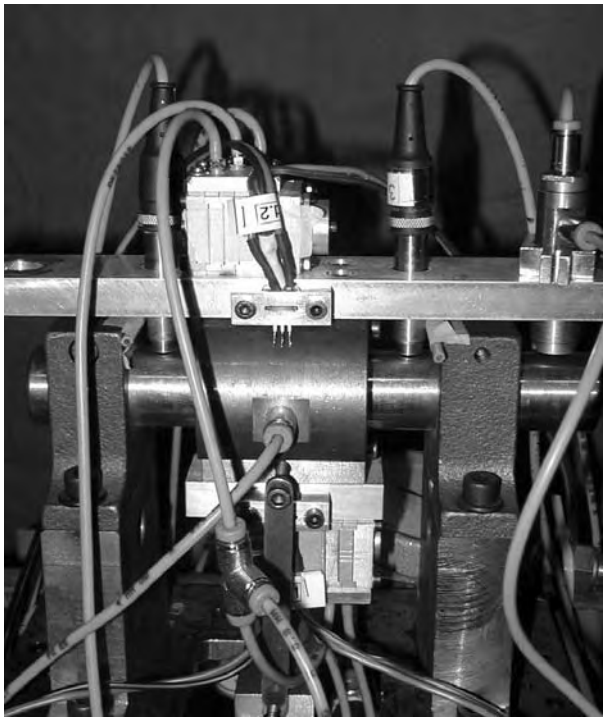

Fig. 13: *Test bed for pneumatically controlled air bearings*

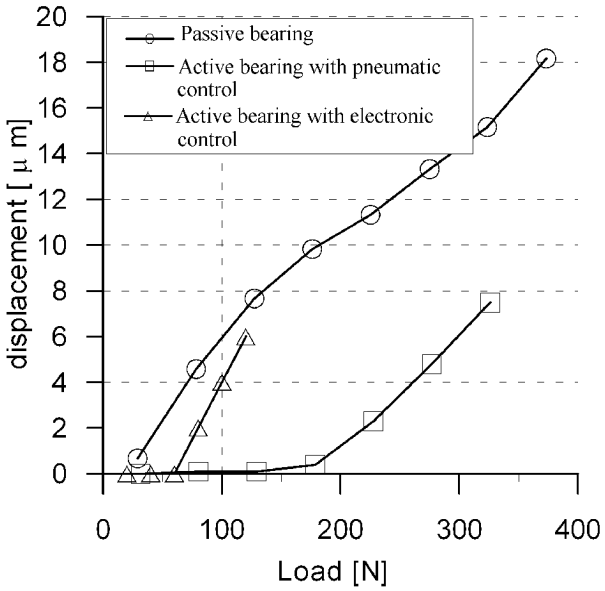

Fig. 14: *Load on pneumo-static bushing v.s. displacement: active and passive behaviour*

3 Variable-Profile Linear Guideways

Pneumatic cylinders can be adapted for frictionless linear positioning by eliminating the conventional seals and using an appropriate profile configuration for the moving element, or piston.

The working principle of variable-profile linear guideways is the same as air bearings. Low radial displacements allowed by strict tolerances are measured by the same micrometric displacement sensors used in air bearings test benches.

A small leakage flow passes from the pressurized chamber to a discharge chamber along the guideway direction of movement through a thin air gap between the moving and stationary elements. The special piston configuration enables a self-centering force to form which prevents stick-slip between the parts in relative motion.

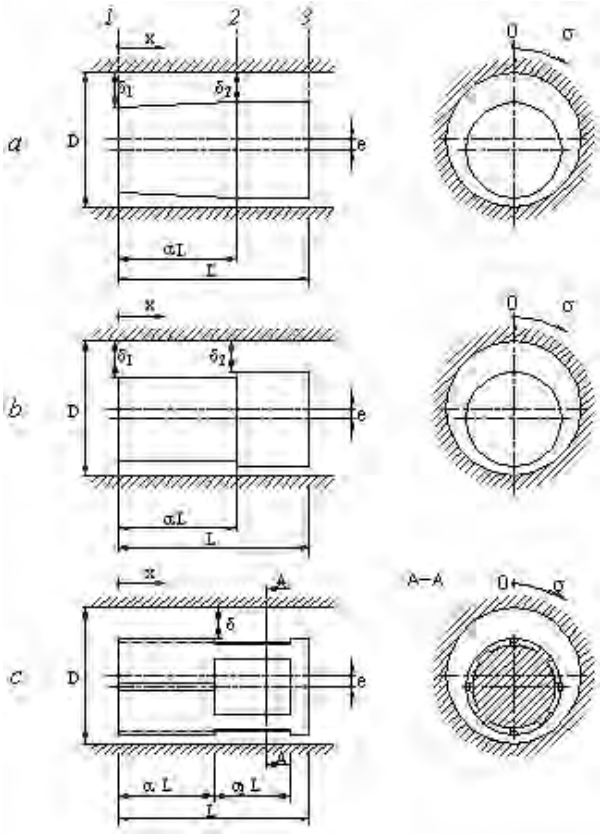

Fig. 15: *Sealless piston geometries: a, tapered; b, step; c, slot-pocket*

When the cylinder is supplied, aerostatic support is guaranteed even when piston movement stops. Figure 15 shows the three different pneumatic cylinder piston geometries developed for this purpose, viz.: *a* tapered, *b* stepped, *c* slot-pocket. In the figure, piston length is designated as L and barrel diameter as D; α is the percentage of length before the discontinuity section, while for the type *c* piston, α_1 designates the percentage of pocket length. In addition, δ_1, δ_2 are the radial thicknesses of the air gap in sections 1,2; for the type *c* piston, $\delta_1 = \delta_2 = \delta$.

To validate the theory applied to these systems, prototype pistons with the geometries described above

were constructed, along with a test bench whereby axial and circumferential pressure distribution and consumed flow rate can be measured while varying the eccentricity between the piston and the barrel, see Belforte (2005). For all three piston geometries, D = 50 mm and L =100 mm. For types *a)* and *b)*, three prototypes were made with α = 0.4, 0.6, 0.8, while for type *c)*, a further three prototypes were constructed with α = 0.3, 0.5, 0.7 and α_1 = 0.6, 0.4, 0.2.

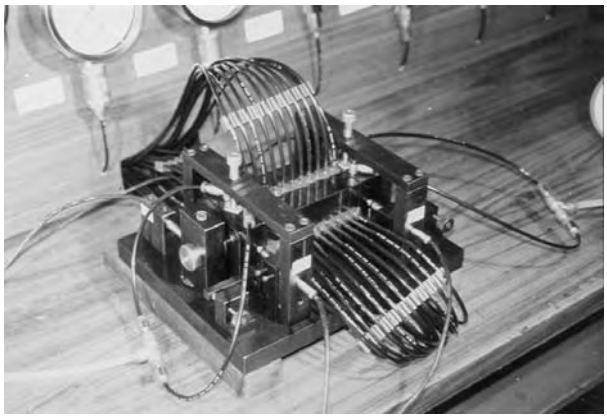

Fig. 16: *Sealless piston test bed*

Subscript *0* in δ_0 designates coaxial conditions for piston and barrel. Air gap heights δ_{10}, δ_{20} are approximately 40 μm and 20 μm for pistons *a* and *b*, and are 20 μm for piston *c*. Pressure was measured at pressure taps spaced at equal distances along the piston axis and around the circumference. Figure 16 is a photograph of the test bench in which the piston, the exterior of the barrel, the pressure taps and the lines connecting the latter to the pressure gauges can be seen. The piston is secured via a precision mount to a plate so that its axis is parallel to the bench base plane. Relative piston-barrel position can be precisely adjusted by means of an arrangement of screws and multiplying linkages as shown schematically in Fig. 17. The barrel can be moved by turning screws A and B, which engage blocks positively connected to the base plate.

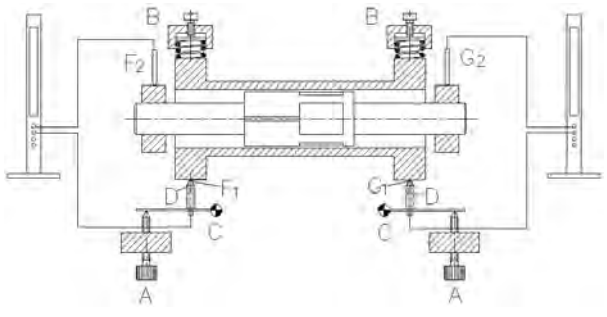

Fig. 17: *Sealless piston test bench equipped with screws and multiplying linkages*

The lever linkages, which pivot at C, demultiply the displacement thus imparted, transmitting it to the barrel at support points D. Displacements are measured by means of four electronic position transducers (F_1, F_2, G_1, G_2) positioned in pairs on the ends of the piston and barrel. An example of axial pressure distribution for the slot-pocket piston under particular eccentricity conditions and relative supply pressure of 0.6 MPa is shown in Fig. 18. Experimental data refer to angular positions $\sigma = 0$ and $\sigma = \pi$, and are compared with those obtained by applying the theory of one-dimensional flow in thin air gaps.

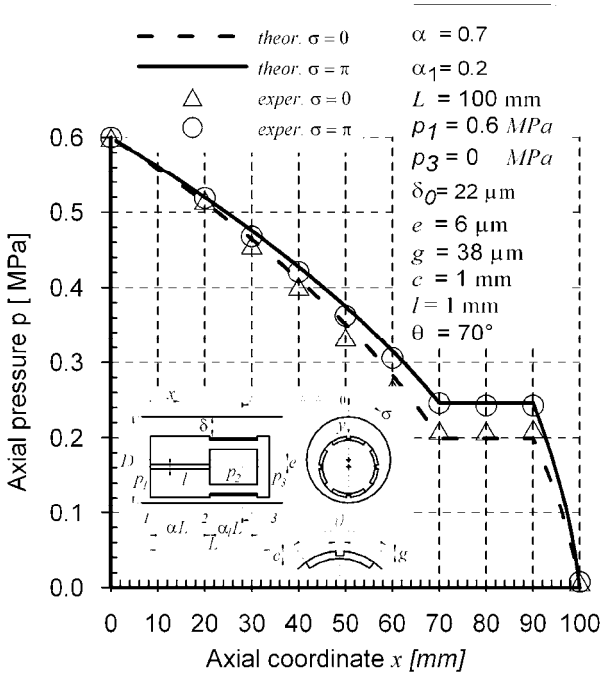

Fig. 18: *Slot-pocket piston; experimental and theoretical axial pressure distribution*

4 Dynamic and Hybrid Air Bearings

Dynamic air bearings have no external air pressure supply. Their load carrying capacity is due to rotation; in some cases they are plain bearings, while in other cases one of the surfaces is profiled. When it is also necessary to ensure load carrying capacity at low or null rotational speeds, e.g., during starts and stops, external pressurized air is provided. In this case, the air bearings are referred to as hybrid, and load capacity is achieved without profiled clearances.

Figure 19 is a cutaway view of a pneumatic spindle with hybrid gas bearings, see Belforte et al. (2006C).

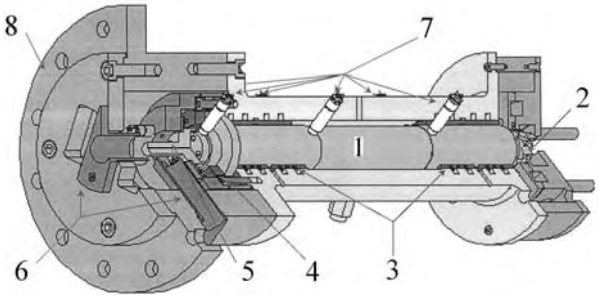

Fig. 19: *Sketch of the pneumatic spindle*

The rotor (1), approximately 500 mm long with a 50 mm diameter, is driven by an air turbine (2) and carried on two radial bushings (3) and a thrust bearing (4). Radial and axial clearances are 20 and 15 micron respectively. The rotor can be loaded radially or axially

on its end (5), called nose, by suitable load devices (6). The latter make it possible to measure axial and radial stiffness. The spindle is mounted vertically via flange (8) on a base, and rotor position is monitored by four capacitive displacement transducers (7) facing the rotor radially. Transducers have 0.1 micron resolution, 0-0.5 mm measuring range and 6 kHz passband. It is possible to determine whether whirl is conical or cylindrical. Thermocouples inserted in the housing measure the temperature of the discharged air and the housing surface.

An optical tachometer faces the turbine and measures spindle rotational speed.

Figure 20 shows the pneumatic circuit, consisting of three supply lines for the bearings (1), the load devices (2) and the turbine (3). Lines are provided with two air filtration units in series (4) whose filtration efficiency is 93 % and 99.99 % with 0.1 micron diameter particles. Air flow rates are measured by flow meters (5).

A reservoir in the bearing supply line prevents damage should the air supply fail without warning, as it allows the rotor to decelerate.

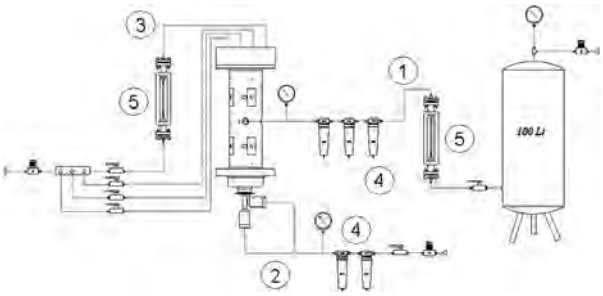

Fig. 20: *Air supply system of the pneumatic spindle*

The prototype was designed to obtain tool stiffness comparable to that of common industrial spindles (30 N/micron), and was tested up to 60000 rpm. Figures 21a and 21b show experimental radial and axial load capacity on the nose respectively for different bearing supply pressures.

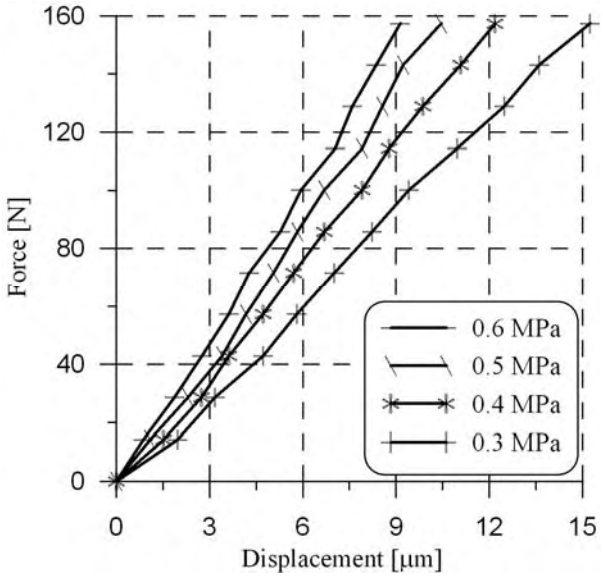

Fig. 21a: *Radial stiffness on the nose*

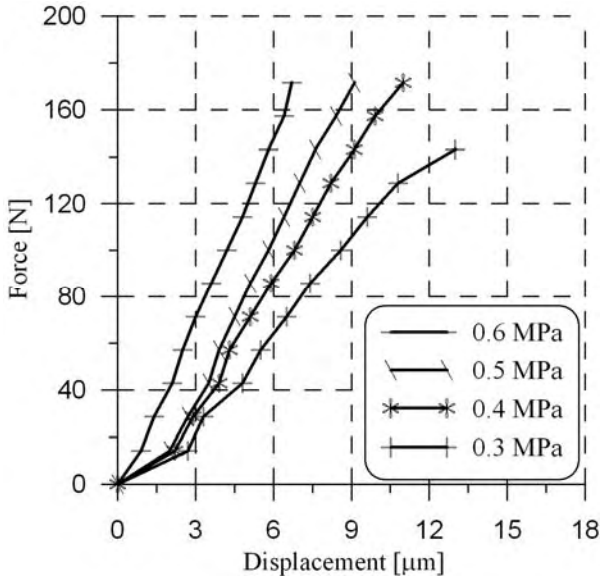

Fig. 21b: *Axial stiffness on the nose*

Figure 22 shows a similar spindle driven by an asynchronous motor with closed loop speed control, see Belforte et al. (2007D). The nominal power is 2.5 kW and speed is 75000 rpm. A tool can be mounted to test the electrospindle during the machining process. Motor and discharge air temperatures are controlled by a closed cooling circuit.

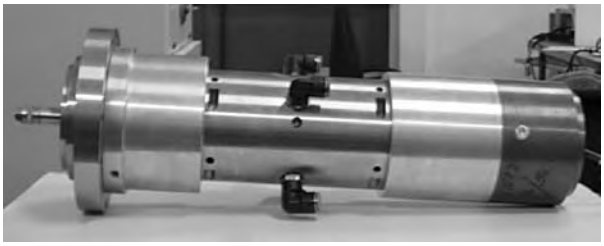

Fig. 22: *Pneumatic electrospindle*

Rotor orbits on the motor side measuring plane at different rotational speeds are shown in Fig. 23. They are measured with the same capacitive displacement transducers used for the pneumatic spindle.

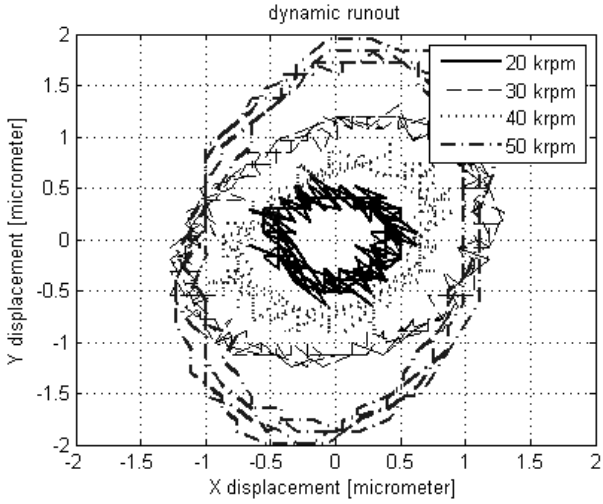

Fig. 23: *Electrospindle radial displacement on motor side measuring plane, at different rotational speeds*

Other studies are performed on applications where high stiffness is not required, but whirl stability must be improved. In particular, a spindle of diameter 37 mm with air bearings and pneumatic turbine was designed for textile applications, as is visible in Fig. 24, see Belforte et al. (2006B).

In this case, the bushing is mounted so that it floats on rubber o-rings of cross-section diameter 1.78 mm (see the enlargement) which introduce a damping action into the system and make it possible to operate at lower supply pressures than those for fixed air bearings. In addition to introducing a damping action, the rubber rings provide a seal between supply and discharge slots. With the compliant supports, it was also possible to investigate the whirl stability threshold experimentally without damaging the rotor and the bushing. Figure 25 shows rotor trajectories with self-excited whirl, measured on two planes, one on the turbine side, the other on the nose side. The sensors used (capacitive displacement transducers) are visible in Fig. 24, facing the rotor and the bushing. This spindle was rotated up to 75 krpm and the influence of the dynamic properties of rubber on whirl stabilization was evaluated.

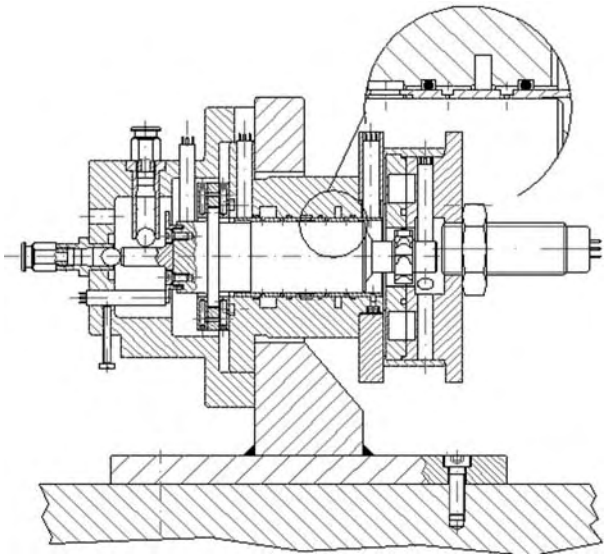

Fig. 24: *Sketch of spindle with bushing mounted floating on O-rings*

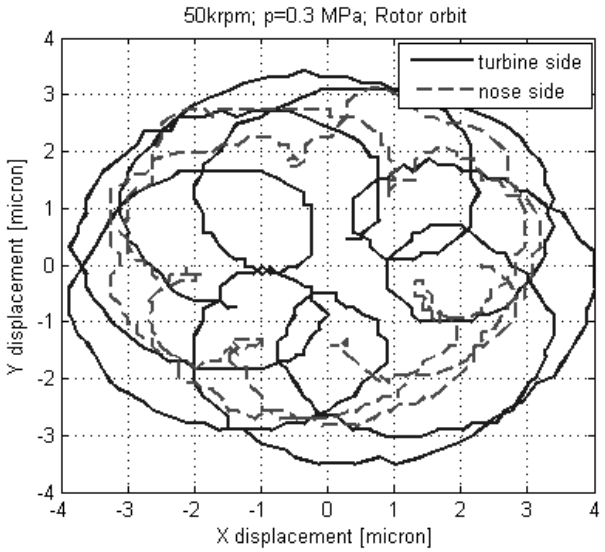

Fig. 25: *Rotor radial displacement near instability*

An ultra-high speed spindle with 10 mm diameter bearings capable of rotational speeds up to 300000 rpm was recently developed. To achieve stable behavior, bearing geometry was modified to feature an elliptical bushing bore. Though this entails greater manufacturing challenges, it increases the bearing's stability.

5 Conclusions

This article presented several types of air bearing and frictionless linear positioning systems investigated at the Politecnico di Torino Department of Mechanics. Particular attention was devoted to the test benches used to evaluate their performance. Testing was aimed at improving parameters such as stability, stiffness and air consumption, requirements for which vary according to application. A major effort went into selecting instruments with the appropriate degree of precision for measuring these parameters during testing, as well as for checking dimensions and geometry of the systems under investigation. The instrumentation used to measure air gap height received special attention in order to ensure repeatable results, carrying out calibration procedures for the sensors mounted directly on the test benches.

Experimental testing plays an essential role in supporting and improving numerical simulations, as well as in the development of new theoretical models. It lays the foundations for reliable numerical and analytical models which can be put to practical use in designing systems of this kind.

Current work at the Department focuses on improving parameters such as stability and stiffness, and on reducing consumption. This involves both experimental work and theoretical investigation based on simulations: efforts that are complementary, as experimental test benches serve to build and improve theoretical models, while the models, once fine-tuned, make it possible to save time in designing new solutions.

References

Belforte, G., **Raparelli, T.**, **Mazza, L.** and **Trivella, A.** 2005. Analysis, design and comparison of different types of pistons for sealless pneumatic cylinders and valves. *Tribology Transactions*, Vol. 48, pp. 377-388.

Belforte, G., **Raparelli, T.**, **Trivella, A.**, **Viktorov, V.** and **Visconte, C.** 2006A. Numerical analysis on the supply hole discharge coefficient in aerostatic bearings. *5th AIMETA International Conference on Tribology*, September 20-22, Parma, Italy.

Belforte, G., **Raparelli, T.**, **Viktorov, V.** and **Colombo, F.** 2006B. An experimental study on a high-speed rotor supported by air bearings mounted on O-rings. *Proceedings of the 8th biennal ASME Conference on Engineering System Design and Analysis ESDA* 2006, Torino, Italy, 4-7 July.

Belforte, G., **Raparelli, T.**, **Viktorov, V.** and **Trivella, A.** 2002. Analysis of steady and transient characteristics of pneumatic controlled air bearing. *5th JFPS International Symposium on Fluid Power*, Nara, Japan, November 12-15, edited by S. Yokota.

Belforte, G., **Raparelli, T.**, **Viktorov, V.** and **Trivella, A.** 2007A. Fine metal wire mesh feeding system for aerostatic pads. *European Conference on Tribology ECOTRIB 2007*. June 12-15, Vol. 1, pp. 563-573.

Belforte, G., **Raparelli, T.**, **Viktorov, V.** and **Trivella, A.** 2007B. Permeability and inertial coefficients of porous media for air bearing feeding systems. *Journal of Tribology*, October, Vol. 129, pp. 705-711.

Belforte, G., **Raparelli, T.**, **Viktorov, V.** and **Trivella, A.** 2007C. Discharge coefficients of orifice-type restrictor for aerostatic bearings. *Tribology International*, Vol. 40, pp. 512-521.

Belforte, G., **Raparelli, T.**, **Viktorov, V.**, **Trivella, A.** and **Colombo, F.** 2006C. An experimental study of high-speed rotor supported by air bearings: test rig and first experimental results, *Tribology International*, Vol. 39, pp. 839-845.

Belforte, G., **Raparelli, T.**, **Viktorov, V.**, **Trivella, A.** and **Colombo, F.** 2007D. Study of a high speed electrospindle with air bearings. *European Conference on Tribology ECOTRIB 2007*. June 12-15, Vol. 2, pp. 969-982, Ljubliana, Slovenia.

Boffey, D. A. and **Wilson, P. M.** 1981. An experimental Investigation of the Pressures at the Edge of a Gas Bearing Pocket. *Journal of Lubrication Technology*, Vol. 103, pp. 593-600.

Boffey, D. A. and **Desai, D. M.** 1980. An experimental investigation into the rubber-stabilization of an externally-pressurized air-lubricated thrust bearing, *ASME Trans., Journal of lubrication technology*, Vol. 102, pp. 65-70.

Cameron, A. 1971, Basic lubrication Theory, Longman, London.

Crabtree, A. B., **Manring, N. D.** and **Johnson, R. E.** 2005. Pressure measurements for translating hydrostatic thrust bearings, *International Journal of Fluid Power,* Vol. 6, No 3, pp. 19-24.

Czolczynski, K. 1994. Stability of flexibly mounted self acting gas journal bearings*, Nonlinear Science,* Part. B, Vol. 7*, Chaos and Nonlinear Mechanics*, pp. 286-299 (World Scientific, Singapore).

Constantinescu, V. N., **Nica, A.**, **Pascovici, M. D.**, **Ceptureanu, G.** and **Nedelcu, S.** 1985. Sliding bearings. Allerton Press, New York.

Gross, W. A., **Matsch, L. A.**, **Castelli, V.**, **Eshel, A.**, **Vohr, J. H.** and **Wildmann, M.** 1980. Fluid film lubrication, Wiley, New York.

Raparelli, T., **Viktorov, V.**, **Manuello, A.** and **Trivella, A.** 2000. Air bearing with pneumatic active control. *2000 AIMETA International Tribology Conference*, L'Aquila, Italy, September 20-22, pp. 693-700.

Raparelli, T., **Viktorov, V.**, **Trivella, A.** 1998. Static and dynamic analysis of pneumatic support. *7th International Workshop on robotics in Alpe-Adria Danube region-RAAD 98. Smolenice Castle*, Slovakia, June 26-28, pp. 405-410.

Federico Colombo
Born in 1977, he graduated in Mechanical Engineering (2001) at the Politecnico di Torino, Italy, discussing the experimental thesis *"A new gripper with piezoceramic actuators"*. In April 2006 he received PhD in Applied Mechanics from the Politecnico di Torino. His doctorate and post-doc. research involves pneumatic systems and in particular gas bearings.

Andrea Trivella
He graduated in mechanical engineering, Italy, in 1993. At the present he is researcher in Applied Mechanics at the Politecnico di Torino. His research activity concerns fluid automation and tribology, in particular pneumatic systems, fluidic components and gas bearings.